

## A simple plane-strain solution for functionally graded multilayered isotropic cylinders

E. Pan<sup>†</sup>

Department of Civil Engineering, The University of Akron, Akron, OH 44325-3905, USA

A. K. Roy<sup>‡</sup>

Air Force Research Laboratory, Materials and Manufacturing Directorate, AFRL/MLBC,  
2941 P St., WPAFB, OH 45433-7750, USA

(Received April 7, 2006, Accepted July 11, 2006)

**Abstract.** A simple plane-strain solution is derived in this paper for the functionally graded multilayered isotropic elastic cylinder under static deformation. The solution is obtained using method of separation of variables and is expressed in terms of the summation of the Fourier series in the circumferential direction. While the solution for order  $n=0$  corresponds to the axisymmetric deformation, that for  $n=2$  includes the special deformation frequently utilized in the upper and lower bounds analysis. Numerical results for a three-phase cylinder with a middle functionally graded layer are presented for both axisymmetric ( $n=0$ ) and general ( $n=2$ ) deformations, under either the traction or displacement boundary conditions on the surface of the layered cylinder. The solution to the general deformation case ( $n=2$ ) is further utilized for the first time to find the upper and lower bounds of the effective shear modulus of the layered cylinder with a functionally graded middle layer. These results could be useful in the future study of cylindrical composites where FGMs and/or multilayers are involved.

**Keywords:** elasticity; analytical solution; micromechanics; functionally graded material; fiber/matrix bond; effective modulus; three-phase cylinder.

---

### 1. Introduction

Functionally graded materials (FGMs) are continuously playing an important role in the design of composite structures. Besides their well-known applications in thermal coatings for high temperature resistance, FGMs can be utilized as transition layers to reduce the sharp contrast in the material properties between the laminates (i.e., Zhu *et al.* 1996, Yang and Munz 1997).

To assist the design of FGMs, various modeling and simulation methods have been proposed, including both numerical and analytical approaches (i.e., Aihara *et al.* 1998, Jin *et al.* 2002). While many analytical results have been reported so far, they are mostly associated with plate geometry only (i.e., Pan 2003, Zhong and Shang 2003, Pan and Feng 2005). To the best of the authors'

---

<sup>†</sup> Associate Professor, Corresponding author, E-mail: [pan2@uakron.edu](mailto:pan2@uakron.edu)

<sup>‡</sup> Ph.D., Research Leader, E-mail: [Ajit.Roy@wpafb.af.mil](mailto:Ajit.Roy@wpafb.af.mil)

knowledge, the corresponding FGM cylindrical composite has not been fully investigated except for some simple deformation cases (Horgan and Chan 1999, Alshits and Kirchner 2001, Tarn 2001, Oral and Anlas 2005).

The present study was motivated by recent experimental work on fiber reinforced composites where it was observed that an FGM interface exists between the fiber and the matrix (Lafdi 2005). As such, from the fabrication and design points of view, it would be helpful if one could understand the effect of different FGMs on the distribution of the displacement, strain, and stress. The ability to estimate the effective material property is also an important issue in the corresponding FGM cylindrical composites. In this paper, we first present the general solution for the FGM cylinder layer by virtue of the method of separation of variables where the  $\theta$ -dependent solution in the circumferential direction is expressed in terms of the Fourier series. For multilayered FGM cylinders, a system of linear equations are formed, which can be solved for the given boundary conditions. We discuss further in detail the cases which correspond to the axisymmetric deformation ( $n=0$ ) and the deformation of order  $n=2$  which has been frequently used in the upper and lower bounds analysis. We point out that our formulation for the upper and lower bounds of the shear modulus is presented based on a very simple approach associated with the strain energy and can be for both multilayered and FGM cases. As examples, numerical results on the displacement, strain, and stress are presented for the three-phase cylinder with a FGM middle layer. The analysis shows clearly the influence of the FGM layer on the field distribution in the inner and outer homogeneous layers as well as in the FGM layer. The corresponding effective shear moduli for the three-phase cylinder with FGM middle layer or with homogeneous middle layer are also predicted for the first time based on the solution. Results in this paper could be useful in future numerical study of the layered FGM cylindrical composites based on either boundary or finite element method.

The paper is organized as follows: In Section 2, the general solution for the multilayered FGM cylinder is derived based on the method of separation of variables. In Section 3, the upper and lower bounds formulation is presented for the FGM and multilayered cylinder, which is based on the simple energy equivalence in the radial direction only. Numerical examples are presented in Section 4 to show the influence of the FGM layer on displacement, strain, and stress fields as well as on the upper and lower bounds. Finally, conclusions are drawn in Section 5.

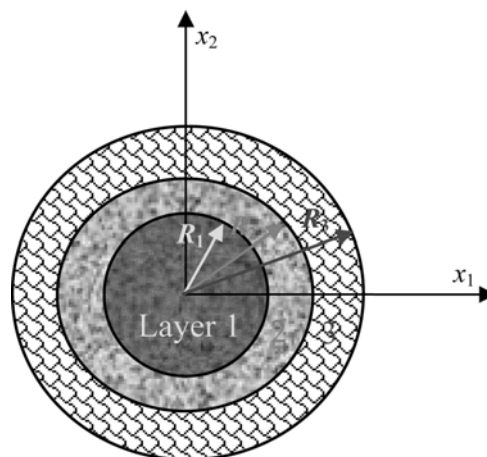


Fig. 1 A three-phase FGM composite cylinder

### 2. General solutions for the multilayered FGM cylinder

Assume that a layered cylinder consists of  $L$  layers, which can be homogeneous or FGM (a three-layered cylinder is shown in Fig. 1). The layered cylinder is solid so that it includes the inner most layer ( $r = 0$ )  $j = 1$ . For any layer  $j$  of the cylinder bounded by  $r = R_{j-1}, R_j$  ( $R_j > R_{j-1}$ ), we assume the Young's modulus as a function of radius in the form of

$$E_j(r) = E_{0j} \left( \frac{r}{R} \right)^k \tag{1}$$

where  $R$  is a nominal length within the layer  $j$ ,  $k$  is the FGM factor which characterizes the variation of the Young's modulus within the layer, and  $E_{0j}$  is the proportional constant.

To find the general solution for each layer, we utilize the method of separation of variables with Fourier series in the  $\theta$ -direction (as a summation from 0 to a large but finite  $N$ ). In other words, we assume that the displacement, strain, and stress fields can be expressed as

$$u_r(r, \theta) = \sum_{n=0}^N u_{rn}(r) e^{in\theta}; \quad u_\theta(r, \theta) = i \sum_{n=0}^N u_{\theta n}(r) e^{in\theta} \tag{2}$$

$$\varepsilon_r(r, \theta) = \sum_{n=0}^N \varepsilon_{rn}(r) e^{in\theta}; \quad \varepsilon_\theta(r, \theta) = \sum_{n=0}^N \varepsilon_{\theta n}(r) e^{in\theta}; \quad \gamma_{r\theta}(r, \theta) = i \sum_{n=0}^N \gamma_{r\theta n}(r) e^{in\theta} \tag{3}$$

$$\sigma_r(r, \theta) = \sum_{n=0}^N \sigma_{rn}(r) e^{in\theta}; \quad \sigma_\theta(r, \theta) = \sum_{n=0}^N \sigma_{\theta n}(r) e^{in\theta}; \quad \tau_{r\theta}(r, \theta) = i \sum_{n=0}^N \tau_{r\theta n}(r) e^{in\theta} \tag{4}$$

where  $i = \sqrt{-1}$ , and the shear stress  $\tau_{r\theta}$  is also represented alternatively as  $\sigma_{r\theta}$ . We remark that while  $n = 0$  corresponds to the axisymmetric deformation,  $n = 2$  corresponds to the case used most frequently in the upper and lower bounds moduli estimation for three-phase composites (i.e., Christensen and Lo 1979, Qiu and Weng 1991). It is emphasized, however, that the solution presented here is more general, which includes multilayered FGMs with the formulation being very simple. For example, in order to solve the general problem in the  $r$ - $\theta$  space, it is sufficient for us to look at the corresponding amplitude of the field quantities for the given order  $n$  (or the  $r$ -dependent function only). Keeping this in mind, the strain-displacement relations and the equilibrium equations in terms of the amplitudes are then reduced to (being functions of the variable  $r$  only)

$$\varepsilon_{rn} = du_{rn}/dr; \quad \varepsilon_{\theta n} = u_{rn}/r - nu_{\theta n}/r \tag{5}$$

$$\gamma_{r\theta n} = nu_{rn}/r + du_{\theta n}/dr - u_{\theta n}/r$$

$$d\sigma_{rn}/dr - n\tau_{r\theta n}/r + (\sigma_{rn} - \sigma_{\theta n})/r = 0 \tag{6}$$

$$d\tau_{r\theta n}/dr + n\sigma_{\theta n}/r + 2\tau_{r\theta n}/r = 0$$

The constitutive relation between the stress and strain is similar to the well-known Hooke's law with the exception that the Young's modulus is now a function of the radius  $r$ .

Eqs. (5) and (6), combined with the isotropic constitutive relation, can be used to solve the unknown amplitudes of the displacement, strain, and stress fields. More specifically, in order to find

the amplitude of the displacement field in each FGM layer, we assume the  $n$ -th order solution as

$$\begin{bmatrix} u_{rn}(r) \\ u_{\theta n}(r) \end{bmatrix} = \begin{bmatrix} c_1 \\ c_2 \end{bmatrix} r^p \quad (7)$$

where the unknown factor  $p$  and the corresponding coefficients ( $c_1$  and  $c_2$ ) can be solved from the following eigensystem of equations:

$$\begin{aligned} & \{2(k+p-1)[(1-\nu_j)p+\nu_j]-n^2(1-2\nu_j)+2(1-2\nu_j)(p-1)\}c_1 \\ & + \{-2\nu_j n(k+p-1)-n(1-2\nu_j)(p-1)+2n(1-2\nu_j)\}c_2 = 0 \\ & \{n(1-2\nu_j)(k+p-1)+2n(\nu_j p+1-\nu_j)+2n(1-2\nu_j)\}c_1 \\ & + \{(1-2\nu_j)(k+p-1)(p-1)-2n^2(1-\nu_j)+2(1-2\nu_j)(p-1)\}c_2 = 0 \end{aligned} \quad (8)$$

where  $\nu_j$  is the Poisson's ratio of the layer  $j$ , and  $k$  again characterizes the FGM as given in Eq. (1). For any layer other than the inner layer ( $r=0$ ), there are generally four different (complex) roots  $p_m$  with four different (complex) pairs of eigenvectors ( $c_{1m}$ ,  $c_{2m}$ ) (see Appendix A for detailed discussion). Therefore, the amplitudes of the displacements can be obtained as

$$\begin{bmatrix} u_{rn}(r) \\ u_{\theta n}(r) \end{bmatrix} = \text{Re} \sum_{m=1}^4 b_m \begin{bmatrix} c_{1m} \\ c_{2m} \end{bmatrix} r^{p_m} \quad (9)$$

where Re stands for the real part of the complex function. Once the displacement amplitudes are found, amplitudes of the strains are obtained using the displacement-strain relation, and stresses using the constitutive relation. It is obvious that for the solution to be bounded for the inner layer ( $r=0$ ), it is necessary to choose solutions corresponding to the two roots which have a positive real part.

Once the general solution for each layer is derived, the boundary condition as well as the interface condition can be applied to solve all the unknowns involved in the layered cylinder (assuming continuity of the displacement and traction vectors at the interfaces between adjoining layers). The size of the system of linear equations will be proportional to the number of layers. Alternatively, it is possible to find the propagator matrix for each layer and then propagate the solutions from layer to layer (i.e., Pan 1997) to arrive at a system of equations involving only 2 unknowns. The propagator matrix (or transfer matrix) has been utilized previously in many areas including those related to laminate FGM composites (e.g., Pan 2001, 2003, Pan and Han 2005). In this paper, however, the direct solution method is adopted as the number of layers studied here is relatively small.

### 3. Upper and lower bounds of the effective shear modulus for multilayered FGM cylinders

In this section, we follow the general procedure as in Christensen and Lo (1979) and Qiu and Weng (1991) for three-phase composites in order to find both the upper and lower bounds of the effective shear modulus for multilayered FGM cylinders. It can be observed that the formulation

presented here is extremely simple with all the calculations in the radial  $r$ -direction only.

In order to obtain the upper bound, we apply the following displacement condition on the surface of the outer layer  $r = R_L$  (in terms of the Cartesian coordinates  $(x_1, x_2)$  in the  $(r, \theta)$ -plane):

$$\bar{u}_\alpha(r = R_L; \theta) = \bar{\varepsilon}_{\alpha\beta} x_\beta \tag{10}$$

where the described non-zero components of the strain tensor are

$$\bar{\varepsilon}_{11} = -\bar{\varepsilon}_{22} = \bar{\varepsilon} \tag{11}$$

It is easy to show that in terms of the polar coordinates, the displacement boundary condition becomes

$$\begin{bmatrix} \bar{u}_r(r = R_L; \theta) \\ \bar{u}_\theta(r = R_L; \theta) \end{bmatrix} = \bar{\varepsilon} R_L \begin{bmatrix} \cos 2\theta \\ -\sin 2\theta \end{bmatrix} \tag{12}$$

Or in general,

$$\begin{bmatrix} \bar{u}_r(r = R_L; \theta) \\ \bar{u}_\theta(r = R_L; \theta) \end{bmatrix} = \bar{\varepsilon} R_L \begin{bmatrix} e^{2i\theta} \\ ie^{2i\theta} \end{bmatrix} \tag{13}$$

Therefore, the displacement amplitudes of second order ( $n=2$ ) should satisfy the following boundary condition:

$$\begin{bmatrix} \bar{u}_{r2}(r = R_L) \\ \bar{u}_{\theta2}(r = R_L) \end{bmatrix} = \bar{\varepsilon} R_L \tag{14}$$

Again, the subscript “2” on the left-hand side of the equation indicates the amplitude of the displacement corresponding to order  $n=2$ .

Similarly, to find the lower bound, the traction boundary condition on the surface of the outer layer  $r = R_L$  (again, in terms of the Cartesian coordinates) is described by:

$$\bar{t}_\alpha(r = R_L; \theta) = \bar{\sigma}_{\alpha\beta} n_\beta \tag{15}$$

where the described non-zero components of the stress tensor are

$$\bar{\sigma}_{11} = -\bar{\sigma}_{22} = \bar{\sigma} \tag{16}$$

In terms of the polar coordinates, the traction boundary condition becomes

$$\begin{bmatrix} \bar{\sigma}_r(r = R_L; \theta) \\ \bar{\tau}_{r\theta}(r = R_L; \theta) \end{bmatrix} = \bar{\sigma} \begin{bmatrix} \cos 2\theta \\ -\sin 2\theta \end{bmatrix} \tag{17}$$

Or in general,

$$\begin{bmatrix} \bar{\sigma}_r(r = R_L; \theta) \\ \bar{\tau}_{r\theta}(r = R_L; \theta) \end{bmatrix} = \bar{\sigma} \begin{bmatrix} e^{2i\theta} \\ ie^{2i\theta} \end{bmatrix} \tag{18}$$

Therefore, the corresponding traction amplitudes of order  $n=2$  satisfy the following boundary condition:

$$\begin{bmatrix} \bar{\sigma}_{r2}(r = R_L) \\ \bar{\tau}_{r\theta2}(r = R_L) \end{bmatrix} = \bar{\sigma} \quad (19)$$

In both cases, the effective shear modulus  $G_{eff}$  is calculated based on the equivalence of the strain energies between the multilayered FGM model and the homogeneous model with the effective shear modulus. The derivation is presented below:

Since both the multilayered FGM and the homogeneous models have the same  $\theta$ -dependence, multiple factors from integration over the variable  $\theta$  are therefore the same on both sides of the energy equation. Consequently, it is only necessary to carry out the integration along the radial direction. For a linear elastic cylinder made of  $L$  FGM layers, the strain energy is calculated from

$$\begin{aligned} E_{Total} &= \frac{1}{2} \sum_{j=1}^L \int_{R_{j-1}}^{R_j} \sigma_{\alpha\beta2}(r) \varepsilon_{\alpha\beta2}(r) r dr \\ &= \frac{1}{2} \sum_{j=1}^L \int_{R_{j-1}}^{R_j} \left\{ \frac{2G}{1-2\nu} [(1-\nu)(\varepsilon_{r2}^2 + \varepsilon_{\theta2}^2) + 2\nu\varepsilon_{r2}\varepsilon_{\theta2}] + G\gamma_{r\theta2}^2 \right\} r dr \end{aligned} \quad (20)$$

This expression can be used to find energy in the multilayered FGM model once all the coefficients in each layer are solved under the given boundary and interface conditions. The energy for the corresponding homogeneous model with the undetermined effective shear modulus  $G_{eff}$  is evaluated based on simple surface integration where the  $\theta$  integration cancels out when equating this expression to that of the multilayered FGM model in Eq. (20). For the equivalent homogeneous model, the total energy is

$$E = \frac{1}{2} \int \sigma_{\alpha\beta2} \varepsilon_{\alpha\beta2} dV = \frac{1}{2} \int \sigma_{\alpha\beta2} n_{\beta} u_{,\alpha 2} dS \quad (21)$$

Ignoring the  $\theta$ -dependent factor, the effective energy is therefore reduced to

$$E_{eff} = \frac{1}{2} \sigma_{\alpha\beta2} n_{\beta} u_{,\alpha 2} R_L \quad (22)$$

Using either the displacement or traction boundary condition, combined with the solved coefficients for the equivalent model, it can be shown that the expression for the effective energy Eq. (22) involves only the effective shear modulus as the unknown. Letting the effective energy Eq. (22) equal the multilayered FGM energy Eq. (20), then the effective shear modulus  $G_{eff}$  can be finally solved.

## 4. Numerical examples

### 4.1 Example 1: Upper and lower bounds of shear modulus in three-phase cylinders

We first checked our solution of multilayered cylinders for the effective shear modulus. For the

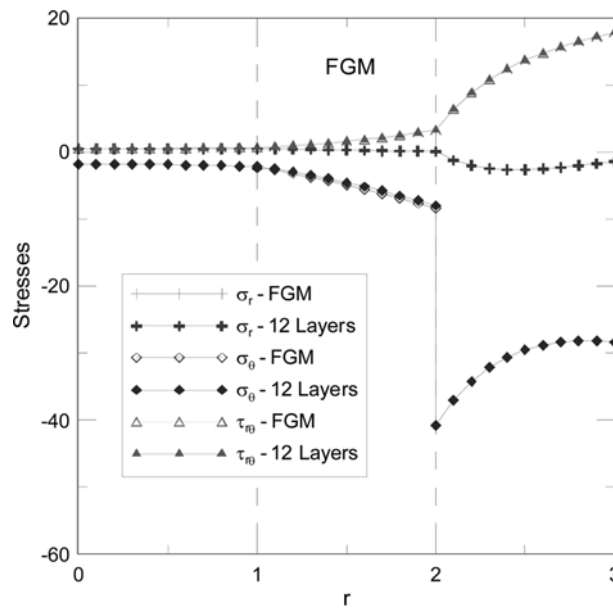


Fig. 2 Comparison of the amplitudes ( $n=2$ ) of stresses based on the FGM vs. discrete layered models under the displacement boundary condition

Table 1 Upper and lower bounds of the effective shear modulus  $G_{eff}$  for the three-phase composite with  $\nu_1 = \nu_2 = \nu_3 = 0.3$  and  $d_2:d_1 = 2:1$

$E_1/E_2/E_3$	Fraction $d_1$	Upper $G_{eff}$	Lower $G_{eff}$
1/5/25	0.1	5.9398	4.0706
	0.2	3.8299	1.8252
	0.3	1.6760	1.0535
25/5/1	0.1	0.60833	0.53305
	0.2	0.99751	0.76440
	0.3	2.1978	1.8029
25/1/5	0.1	1.4395	1.3439
	0.2	1.1406	1.0917
	0.3	0.78148	0.75887

three-phase cylinder case considered in Qiu and Weng (1991), the Young's modulus  $E_i$  in each layer takes a value of 1, 5, or 25 (for example,  $E_1/E_2/E_3 = 1/5/25$  for one of the models), whilst the Poisson's ratio is the same, i.e.,  $\nu_1 = \nu_2 = \nu_3 = 0.3$ . The upper and lower bounds for the shear modulus predicted from our analytical formulation are found to be the same as those in Qiu and Weng (1991, Figs. 1 and 2). For instance, listed in Table 1 are some of the results from our solution for different volumetric fractions  $d_1$  (with fixed  $d_2:d_1 = 2:1$ ). The corresponding radii of the three-phase cylinder are given in Table 2.

Table 2 Volumetric fraction  $d_1$  and the corresponding radii of the three-phase cylinder for fixed ratio  $d_2:d_1 = 2:1$ 

$d_1$	$R_1$	$R_2$	$R_3$
0.1	0.9486833	1.64316767	3.0
0.2	1.3416407865	2.2379	3.0
0.3	1.64316767	2.84604989	3.0

#### 4.2 Example 2: A three-phase cylinder with a middle FGM layer ( $n = 2$ )

The second example is for a three-phase cylinder with a middle FGM layer. Solutions for both the direct FGM and discrete models are employed to carry out the calculation. In the discrete model, a total of 12 layers are used. In other words, 10 discrete homogeneous layers are used to approximate the middle FGM layer (it has been checked that when the number of the discrete layers is equal to 10 or larger, the discrete-based solution is nearly the same as the FGM solution). The FGM factor  $k$  in Eq. (1) is chosen in such a way that  $E_2(r) = (r/R_1)^{2.321928}$  in the FGM layer. Other parameters are  $R_1 = 1.0$ ,  $R_2 = 2.0$ , and  $R_3 = 3.0$ ,  $\nu_1 = \nu_2 = \nu_3 = 0.3$ ,  $E_1 = 1$  and  $E_3 = 25$ . It is obvious that when  $r = R_1$  we have  $E_2 = 1$ , and at  $r = R_2$ , we have  $E_2 = 5$ . The boundary condition applied at  $R_3 = 3.0$  is the displacement condition described by Eq. (14) with  $\bar{\varepsilon} = 1$ . For example, the amplitudes of the stresses from both the direct FGM and discrete homogeneous models are plotted in Fig. 2. It is observed that both models predict very close results to each other. Furthermore, there is a sharp discontinuity for the normal stress  $\sigma_\theta$  across the interface at  $r = 2$  due to the jump of the Young's moduli on both sides of the interface.

We have also compared this FGM model to a couple of discrete homogeneous three-phase models with different combinations of  $E_1/E_2/E_3$ . While the results for the upper and lower bounds are given in Table 3, the amplitudes of the stress components for different models are presented in Figs. 3(a), 3(b), and 3(c) for the traction boundary condition Eq. (19) with  $\bar{\sigma} = 1$ . It is interesting to note from Table 3 that the shear modulus bounds for the FGM case is somewhere between those of the discrete models  $E_1/E_2/E_3 = 1/2/25$  and  $E_1/E_2/E_3 = 1/3/25$ .

From Fig. 3, we first observe that while the normal ( $\sigma_r$ ) and shear ( $\tau_{r\theta}$ ) stresses have approximately the same magnitude, the amplitude of the hoop stress  $\sigma_\theta$  is much larger. For different combinations of  $E_1/E_2/E_3$ , the stress amplitude could decrease in one layer and increase in another for increasing  $E_2$  in the middle layer. For instance, with increasing  $E_2$ , the amplitude of  $\sigma_r$  decreases in layers 1 and 2 but increases in layer 3 (Fig. 3(a)). However, the trend for the FGM layer case is different: while the stress variation for the FGM layer model follows the curve of one of the discrete models  $E_1/E_2/E_3$  in layers 1 and 3, its behavior in the FGM middle layer is different: It

Table 3 Upper and lower bounds of the shear modulus for the FGM middle layer model and the discrete homogeneous models with different combinations of  $E_1/E_2/E_3$ 

$E_1/E_2/E_3$	Upper $G_{eff}$	Lower $G_{eff}$
1/2/25	4.2418	1.8701
FGM	4.4258	2.0653
1/3/25	4.4493	2.2105
1/5/25	4.8311	2.8115

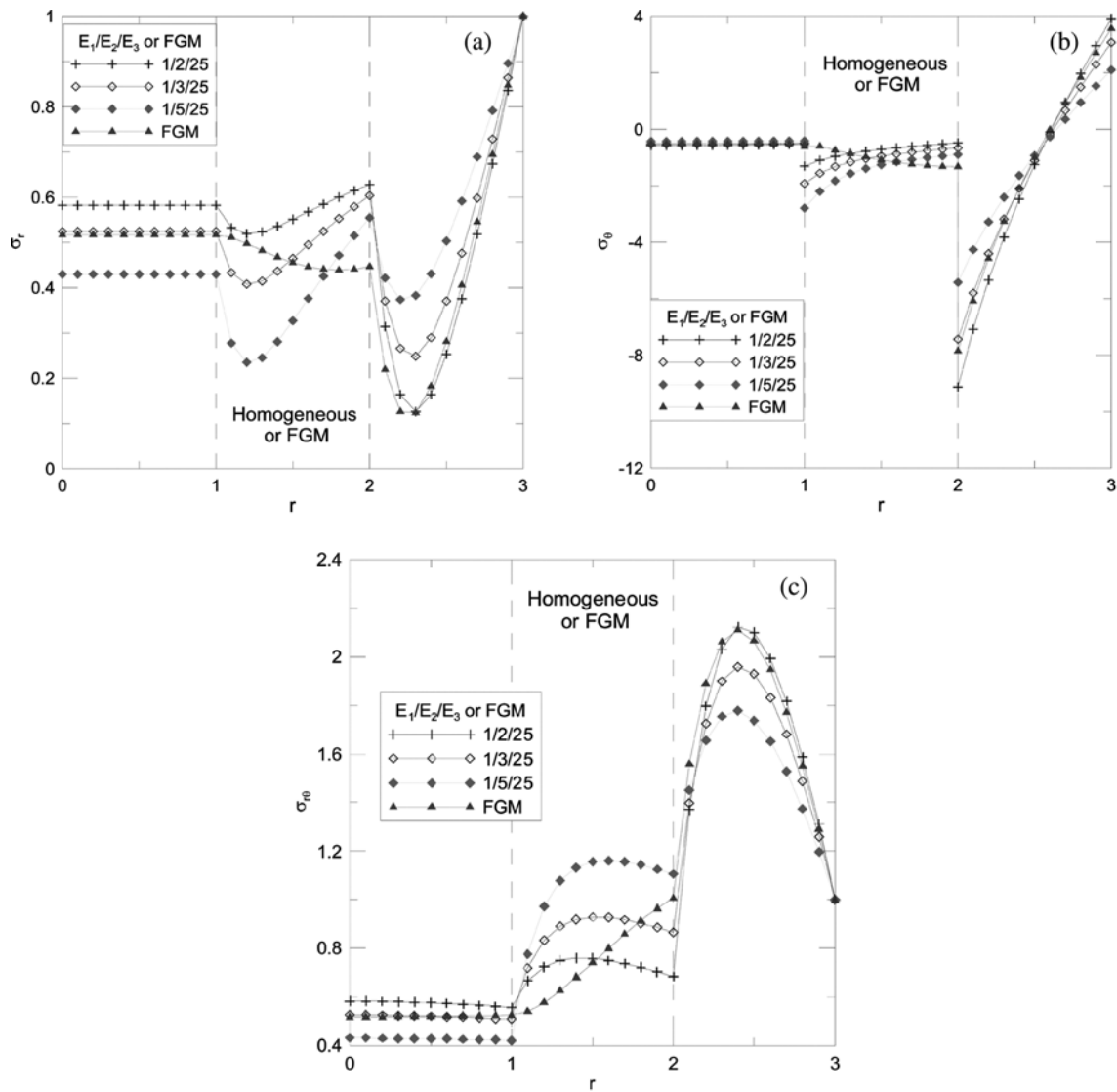


Fig. 3 Amplitudes ( $n=2$ ) of stresses in FGM and discrete layered cylinders under traction boundary condition: Stress  $\sigma_r$  in (a),  $\sigma_\theta$  in (b), and  $\sigma_{r\theta}$  in (c)

crosses some (Figs. 3(a) and 3(c)) or all (Fig. 3(b)) of the curves predicted based on the discrete models  $E_1/E_2/E_3$  in the middle layer. More importantly, the stress variation in the FGM middle layer is much smoother than those in the homogeneous middle layer, and there is no discontinuity for the stress  $\sigma_\theta$  across the interface between the FGM and the inner layer as the Young's moduli is continuous there.

#### 4.3 Example 3: A three-phase cylinder with a middle FGM layer ( $n = 0$ )

The effect of different  $k$  values in the FGM model (Eq. (1)) is studied in this example, where the

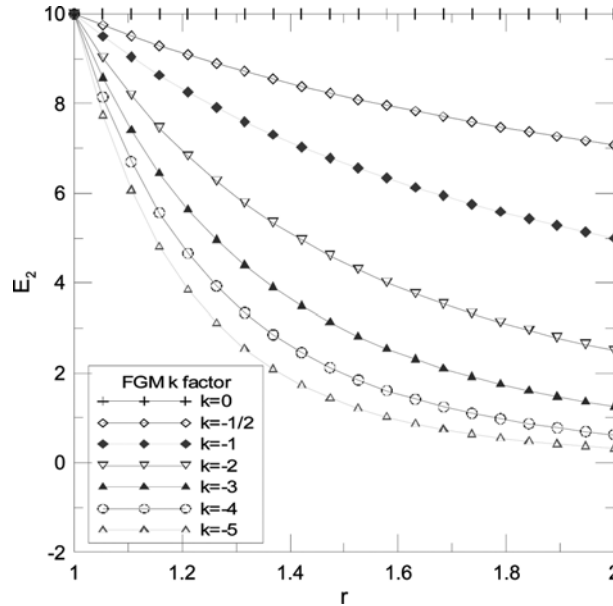


Fig. 4 Young's modulus in the middle FGM layer of a three-phase cylinder

$k$  in the middle FGM layer ( $1 < r < 2$ ) varies as  $k=0, -1/2, -1, -2, -3, -4, -5$ . The deformation is restricted to the axisymmetric case (i.e.,  $n=0$ ) under uniform traction (i.e.,  $\bar{\sigma}_{r0}(r=R_3)=1$ ). While the Poisson's ratios are the same in the three layers (i.e.,  $\nu_1=\nu_2=\nu_3=0.3$ ), the Young's moduli in the inner layer ( $r < 1$ ) and outer layer ( $2 < r < 5$ ) are, respectively,  $E_1=10$  and  $E_3=1$ . The Young's modulus  $E_2$  in the FGM middle layer ( $1 < r < 2$ ) is described by Eq. (1) with  $E_{02}=10$  and its distribution for different  $k$  is plotted in Fig. 4. The corresponding solutions for the displacement, strain, and stress are presented in Figs. 5(a), 5(b), and 5(c). Some interesting features can be observed from Fig. 5:

1) Since the Young's modulus in the inner layer is larger than those in the other two layers, the induced displacement and strain fields in this layer are much smaller. Therefore, the effect of different  $k$  values on the displacement and strain fields within layer 1 ( $r < 1$ ) cannot be clearly observed (Figs. 5(a) and 5(b)).

2) For displacement  $u_r$  (Fig. 5(a)), its values in both the FGM and outer layers increase with increasing magnitude of  $k$ . For strain  $\varepsilon_r$  (Fig. 5(b)), however, with increasing magnitude of  $k$ , its value increases in the FGM layer, but decreases in the outer layer.

3) As for the stress in the inner layer, increasing magnitude of  $k$  corresponds to an increase of the stress value for  $k=0$  to  $-3$ ; however, when  $k=-4$  and  $-5$ , the stress amplitude is reduced, with the result for  $k=-5$  close to that for  $k=-1/2$  (Fig. 5(c)). This feature is possibly due to the fact that for  $k=0$  to  $-3$ , the Young's moduli in the FGM layer are all larger than that in the outer layer; however, for  $k=-4$  and  $-5$ , they become smaller in the FGM layer than that in the outer layer (near  $r=2$  in the FGM layer in Fig. 4).

4) In the outer layer, the stress  $\sigma_r$  decreases with increasing magnitude of  $k$  (Fig. 5(c)).

In general, different  $k$  values have apparent effect on the displacement, strain, and stress in both the FGM middle layer and the outer layer. While the response (displacement, strain, or stress) as a

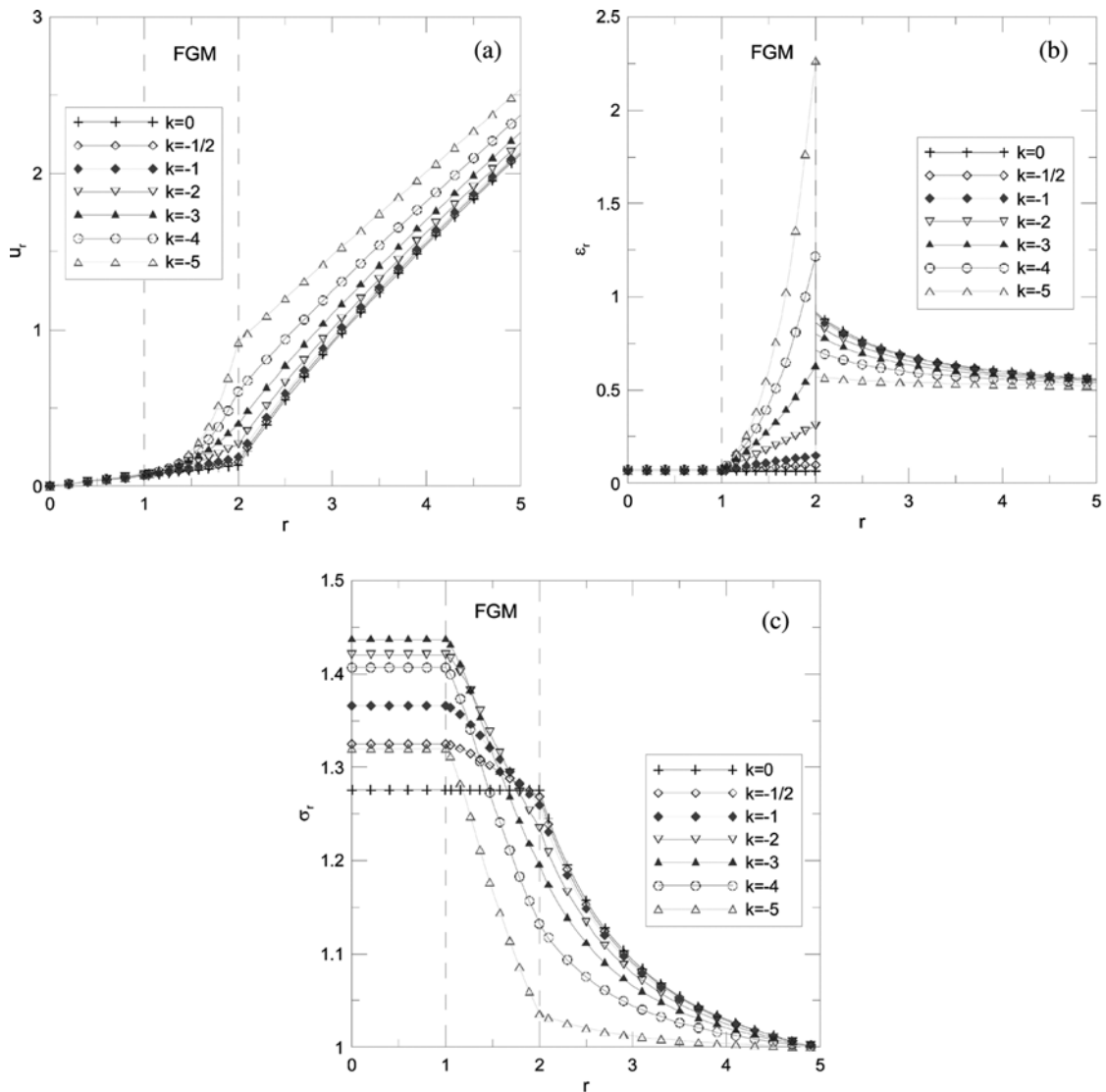


Fig. 5 Amplitudes ( $n=0$ ) of the field quantities for different FGM factors  $k$ : Radial displacement  $u_r$  in (a), strain  $\epsilon_r$  in (b), stress  $\sigma_r$  in (c)

function of  $r$  is gentle in the outer layer, the one in the FGM layer experiences a large change in its amplitude. It is also obvious that, the transfer of the stress from the inner to the outer layer is more complicated than that of the displacement or strain, with the inner fiber carrying most of the stress.

## 5. Conclusions

In this paper, exact solutions are derived for multilayered FGM cylinders under static deformation. They are obtained based on the method of separation of variables and include the previous

axisymmetric solution as a special case. The most commonly used upper and lower bounds formulation is also extended to the general multilayered FGM case and is further presented in terms of a simple energy relation. While our solutions can be applied to many different deformation cases, illustrative results for a three-phase cylinder with a FGM middle layer are presented for orders  $n = 0$  and 2. It is observed clearly that the FGM middle layer can strongly influence the field (displacement, strain, and stress) distribution within the FGM layer and in the inner and outer layers as well. The FGM layer also has an obvious effect on the upper and lower bounds of the effective shear modulus. Results presented in this paper could be useful in future numerical analysis of FGM layered cylinders based on the boundary and finite element methods.

## Acknowledgements

This work was carried out while the first author was at AFRL under the Air Force 2005 Summer Faculty Fellowship Program.

## References

- Aihara, T. Jr., Sho, T. and Kawazoe, Y. (1998), "Molecular dynamics simulation on elastic behavior of Ni/Ni<sub>3</sub>Al interface with graded structure", *J. Japan Institute of Metals*, **62**, 978-985.
- Alshits, V.I. and Kirchner, H.O.K. (2001), "Cylindrically anisotropic, radially inhomogeneous elastic materials", *Proc. R. Soc. Lond.*, **A 457**, 671-693.
- Christensen, R.M. and Lo, K.H. (1979), "Solutions for effective shear properties in three phase sphere and cylinder models", *J. Mech. Phys. Solids*, **27**, 315-330.
- Horgan, C.O. and Chan, A.M. (1999), "The pressurized hollow cylinder or disk problem for functionally graded isotropic linearly elastic materials", *J. Elasticity*, **55**, 43-59.
- Jin, Z.H., Paulino, G.H. and Dodds, Jr. R.H. (2002), "Finite element investigation of quasi-static crack growth in functionally graded materials using a novel cohesive zone fracture model", *J. Appl. Mech.*, **69**, 370-379.
- Lafdi, K. (2005), "TEM characterization of the interface property between the fibre and matrix", *Private Communication*.
- Oral, A. and Anals, G. (2005), "Effects of radially varying moduli on stress distribution of nonhomogeneous anisotropic cylindrical bodies", *Int. J. Solids Struct.*, **42**, 5568-5588.
- Pan, E. (1997), "Static Green's functions in multilayered half-spaces", *Applied Mathematical Modelling*, **21**, 509-521.
- Pan, E. (2001), "Exact solution for simply supported and multilayered magneto-electro-elastic plates", *ASME, J. Appl. Mech.*, **68**, 608-618.
- Pan, E. (2003), "Exact solution for functionally graded anisotropic elastic composite laminates", *J. Composite Mater.*, **37**, 1903-1920.
- Pan, E. and Han, F. (2005), "Exact solution for functionally graded and layered magneto-electro-elastic plates", *Int. J. Eng. Sci.*, **43**, 321-339.
- Qiu, Y.P. and Weng, G.J. (1991), "Elastic moduli of thickly coated particle and fiber-reinforced composites", *J. Appl. Mech.*, **58**, 388-398.
- Tarn, J.Q. (2001), "Exact solutions for functionally graded anisotropic cylinders subjected to thermal and mechanical loads", *Int. J. Solids Struct.*, **38**, 8189-8206.
- Yang, Y.Y. and Munz, D. (1997), "Reduction of residual stresses in a two dissimilar materials joint by using a functionally graded material", In "Composites and Functionally Graded Materials", *Proc. of the Symposia, ASME International Mechanical Engineering Congress and Exposition*, Dallas, TX, 37-43.
- Zhong, Z. and Shang, E.T. (2003), "Three-dimensional exact analysis of a simple supported functionally gradient

piezoelectric plate”, *Int. J. Solids Struct.*, **40**, 5335-5352.  
 Zhu, J., Yin, Z., Mao, J., Lai, Z., Yang, D., Ning, X. and Li, D. (1996), “Interface structure of ZrO<sub>2</sub>-Ni functionally gradient material”, *Acta Metallurgica Sinica*, **32**, 133-138.

**Appendix A: Roots of the eigensystem of Eqs. (8)**

Using *Mathematica*, the four different roots  $p_m$  ( $m = 1, 2, 3, 4$ ) of the system of Eqs. (8) can be found as (for simplicity, the Poisson’s ratio in layer  $j$ , “ $\nu_j$ ”, has been replaced with “ $\nu$ ”):

$$p_{1 \rightarrow 4} = \frac{-k}{2} \pm \sqrt{\frac{k^2}{4} + \frac{a \pm \sqrt{b}}{2(1 - \nu)}} \tag{A1}$$

where

$$\begin{aligned} a &= 1 + 2n^2(1 - \nu) + (1 + k)(1 - 2\nu) \\ b &= k^2 + 16n^2(1 + \nu^2) + 8n^2(k - 4\nu) - 8kn^2\nu(3 - 2\nu) - 4k^2n^2\nu(1 - \nu) \end{aligned} \tag{A2}$$

We remark that in general the four roots are complex. Therefore, the corresponding eigenvectors ( $c_{1m}, c_{2m}$ ) are also complex. Since the displacement solution is real, one needs to take only the real part of the complex solution.

We discuss below the solutions corresponding to those with special functional gradient  $k$  and Poisson’s ratio  $\nu$  values:

**1)  $k = 0$**

This corresponds to the homogeneous material case. For this case, the four roots  $p_m$  in Eq. (A1) are real, and can be expressed as

$$p_{1 \rightarrow 4} = \pm(n \pm 1) \tag{A3}$$

The same roots can also be easily derived from the governing equations when the material is homogeneous.

**2)  $n = 0$**

This corresponds to the axisymmetric deformation studied in detail in the paper. For the axisymmetric case, the four roots  $p_m$  are

$$p_m = \begin{cases} -k/2 \pm \sqrt{k^2/4 + k + 1}; & m = 1, 2 \\ -k/2 \pm \sqrt{k^2/4 + 1 - k\nu/(1 - \nu)}; & m = 3, 4 \end{cases} \tag{A4}$$

It is obvious that for the regular domain of  $k \leq 0$  and  $0 \leq \nu \leq 1/2$ , all the roots in Eq. (A4) are real.

**3)  $n = 2$**

This corresponds to the special deformation associated with the prediction of the effective shear modulus, as discussed in the paper. For this case,

$$\begin{aligned} a &= 10(1 - \nu) + k(1 - 2\nu) \\ b &= k^2(1 - 16\nu + 16\nu^2) + 32k(1 - 2\nu)(1 - \nu) + 64(1 - \nu)^2 \end{aligned} \tag{A5}$$

It is apparent that for  $n = 2$  and also for other orders, the four roots will be, in general, complex (in pair). For example, for  $\nu = 0.3$ , the four roots are

$$p_{1 \rightarrow 4} = -0.357143 \left\{ 1.4k \pm \sqrt{1.96k^2 + 5.6(7.0 + 0.4k \pm \sqrt{31.36 + 8.96k - 2.36k^2})} \right\} \quad (\text{A6})$$

which, for the special functional gradient  $k = -3$  studied in the paper, become

$$p_m = \begin{cases} 4.09063 \pm 0.564382i; & m = 1, 2 \\ 1.09063 \pm 0.564382i; & m = 3, 4 \end{cases} \quad (\text{A7})$$